Hindawi
Geofluids
Volume 2023, Article ID 9159098, 17 pages
https://doi.org/10.1155/2023/9159098

Research Article

The Damage Induced by Blasting Excavation and Seepage Characteristics of Deep Rock under High Seepage Pressure

Qian Dong[1,2] **Xin Liu**[3] **Hangli Gong**[3] **Yi Luo**[3,4] **Xinping Li**[3,4] **and Liangjun Wang**[5]

[1]*State Key Laboratory of Precision Blasting, Jianghan University, Wuhan 430056, China*
[2]*Hubei Key Laboratory of Blasting Engineering, Jianghan University, Wuhan 430056, China*
[3]*School of Civil Engineering and Architecture, Wuhan University of Technology, Wuhan 430070, China*
[4]*Hubei Key Laboratory of Roadway Bridge and Structure Engineering, Wuhan University of Technology, Wuhan 430070, China*
[5]*China Gezhouba Group Co., Ltd., Wuhan 430070, China*

Correspondence should be addressed to Hangli Gong; hangligong58@whut.edu.cn

Received 6 November 2022; Revised 18 December 2022; Accepted 3 April 2023; Published 18 April 2023

Academic Editor: Yiding Bao

By taking the blasting excavation of a deeply buried karst tunnel in the North Tianshan Mountains in China as research objects, the damage induced by blasting excavation and seepage characteristics of deep rock under high seepage pressure was investigated. The COMSOL Multiphysics® software was adopted to establish a simulation model for the blasting excavation of a deeply buried tunnel. By embedding the stress-damage-seepage multifield coupled constitutive relationship, the mechanism of the influences of factors including blasting load, geostress, and hydraulic pressure of karst caves on the blasting excavation-induced damage to, and seepage characteristic of, the surrounding rocks of the tunnel. The results indicate that blasting excavation in the karst tunnel triggers the damage of surrounding rocks, which consists of blasting-induced damage and unloading damage. The time-history curve of the variable for surrounding rock damage rises and consequently tends to a constant value. With the increases in blasting load, geostress, and hydraulic pressure of karst caves, the degree of damage to surrounding rocks is intensified; an increase in geostress will weaken the effect of blasting-induced damage to rock while increasing rock damage arising from unloading. Meanwhile, the degree of damage to the surrounding rock can affect the seepage velocity of water in the surrounding rock to a certain extent. A strong damage and seepage coupled effect occur in the blasting excavation process of the karst tunnel. The such coupled effect is strengthened little by little with the increases in the degree of surrounding rock damage and hydraulic pressures. The results are expected to provide theoretical guidance for hazard prevention and control of blasting excavation in karst tunnels under high geostress conditions.

1. Introduction

Generally, when the magnitude of geostress in deep rocks is above 10 MPa, a new excavation tunnel surface is formed within about 10 ms during a blasting excavation process, yielding a strain magnitude of 10^{-1}. Dynamic stresses generated by explosive blasting and transient unloading are important factors that trigger rock fracture and loosening [1–3]. However, rocks in high-pressure water-rich zones are inclined to be subjected to the effect of high-pressure seepage. Fissures of rocks, under the effect of the excavation-induced dynamic disturbance, undergo a process evolving from initiation, propagation, and coalescence. This causes deteriorating mechanical properties of surrounding rocks while inducing the enlargement of seepage channels, which promotes the seepage field to further evolve [4–6]. Under the coupled effect of seepage and dynamic loading, the transient water pressure of rock fissures will be largely increased, which enables the fissures to further propagate and leads to structural damage of rock, even directly triggers rock failure [7, 8]. Therefore, it is necessary to study the damage induced by blasting excavation and seepage characteristics of deep rock under high seepage pressure.

A series of studies on the blasting excavation-induced damage of rock under high seepage pressure and seepage problems have been investigated worldwide. Tan et al. [9]

discovered that surrounding rocks that lie between a tunnel and a karst under the excavation-induced dynamic disturbance are more prone to suffer a large deformation and even suffer failures, which calls for special attention to the stability of surrounding rocks. Li et al. [10] programmed a program for analyzing and calculating the seepage and damage of surrounding rocks under dynamic loading to obtain the law of the changes in the radius of the damage zone in surrounding rocks with varying pore water pressure under the restriction of multiple factors. Their results proved that the value of the range of the damage zone in surrounding rocks is positively correlated with pore water pressure. Liu et al. [11] believed that damage evolution is a process by which microcracks evolve from initiation, propagation, and coalescence. They constructed a stress-seepage-damage coupled model characterizing changes in permeability and damage evolution of surrounding rocks in the tunnel excavation process and used seepage theory to deduce an equation for the permeability evolution of surrounding rocks. Huang et al. [12] analyzed distributions of the stress field, seepage field, and damage field of surrounding rocks during the tunnel excavation process by taking water inrush hazards that occurred in fracture zones of a karst tunnel as a research object. Their results indicated that disturbance arising from tunnel excavation leads to the redistribution of the in situ rock stress field and causes the change in the seepage state of surrounding rocks. Zhao et al. [13] studied the influences of spatial distribution characteristics of karst caves' locations on the deformation and seepage field of rocks surrounding tunnels. Yang et al. [14] conducted three-dimensional fluid-solid coupled model tests to explore the evolution law of water inrush in karst caves which were induced by tunnel excavation and varying water pressure in the caves. Yuan et al. [15] simulated the influence of mining disturbance in mines on the faults and rivers in the surrounding area based on the rock fluid-solid coupled theory. The results showed that mining activities can cause further damage to faults and rock bridges, causing increased rock permeability, which may allow mining filed to form a coalesced seepage channel spanning from a river to faults. By considering the fluid-solid coupled effect, Guo et al. [16] investigated the evolution laws of the displacement field and seepage field of rock mass on the layer for preventing water inrush when a tunnel face was close to a high-pressure water-rich karst cavity in tunnel excavation and its critical water inrush characteristics. Huang et al. [17, 18] found the permeability of surrounding rocks after tunnel excavation was finished and increased to one or several orders of magnitudes and analyzed the influences of the thickness of damage zones on tunnel gushing and pore pressure distribution. To sum up, exploring the issues about the damage evolution of surrounding rocks under the coupled effect of dynamic loading and seepage field is of significance to surrounding rock stability as well as water inrush prevention and control of deep rock mass.

The extra-long, deeply buried karst tunnel in the North Tianshan Mountains in Xinjiang Province, China, contains rich water, with some tunnel sections containing rich water. It has a maximum burial depth of 1060 m. The tunnel crosses multiple fault fracture zones and has complex geological tectonics, and the surrounding rocks in the fracture development zone of jointed rock mass contain a large number of soluble rocks, which can lead underground water to accumulate to form a karst cave and produces high seepage pressure in surrounding rock masses. It belongs to a typical deep-buried, high-permeability rock tunnel. In this research, the stress-damage-seepage multifield constitutive model was embedded into COMSOL Multiphysics, and the damage induced by blasting excavation and seepage characteristics of deep rock under high seepage pressure were analyzed. The influence mechanism of blasting load, geostress, water pressure of karst caves on the tunnel blasting excavation-induced damage to, and seepage characteristics of surrounding rocks were discussed. The research results can provide theoretical support and reference for similar deep high-permeability rock mass blasting excavation.

2. Blasting Excavation-Induced Damage and Seepage Characteristics of Surrounding Rocks in the North Tianshan Karst Tunnel

2.1. The Stress-Seepage-Damage Coupled Model. For the deeply buried tunnel under the effect of blasting excavation, a stress-seepage-damage multifield coupled constitutive relationship was established using a Drucker-Prager (D-P) yield criterion-based elastoplastic damage model. This constitutive relationship also considered the effects of water pressure and karst water flow in surrounding rocks in karst caves surrounding the tunnel, on the damage to surrounding rocks. Once the effect of effective stress on rocks under the effect of exerted loads exceeds the strength of rocks, plastic strain tends to occur to rocks, accompanied with damage to a certain degree. An internal variable (herein referring to the equivalent plastic strain) is used to characterize the evolution of the rock damage variable based on the elastoplastic damage theory considering plastic deformation mechanism and stiffness degradation. Previous research indicates that the rock damage variable has a linear relationship with equivalent plastic strain, which can be expressed as an exponential function of equivalent plastic strain [19]. tThe equivalent plastic strain $\bar{\varepsilon}_{\mathrm{p}}$ is calculated as

$$\bar{\varepsilon}_{\mathrm{p}} = \frac{\sqrt{2}}{3}\sqrt{\left(\varepsilon_{\mathrm{p1}} - \varepsilon_{\mathrm{p2}}\right)^2 + \left(\varepsilon_{\mathrm{p2}} - \varepsilon_{\mathrm{p3}}\right)^2 + \left(\varepsilon_{\mathrm{p3}} - \varepsilon_{\mathrm{p1}}\right)^2}, \quad (1)$$

where ε_{p1} denotes the first principal plastic strain; ε_{p2} refers to the secondary principal plastic strain; and ε_{p3} is the third principal plastic strain.

The evolution equation of the corresponding damage variable D is as follows:

$$D = 1 - \exp\left[-\kappa\left(\bar{\varepsilon}^p - \bar{\varepsilon}_0^p\right)\right], \quad (2)$$

where the threshold of the equivalent plastic strain $\bar{\varepsilon}_0^p = 0$, namely, there is damage evolution when the equivalent plastic strain occurs; k represents the positive constant obtained in experiments.

There are pores and microcracks in rocks. It can be assumed that water and rock mass are incompressible material under deep high seepage pressure condition, and the weight of water is neglected, the surrounding rock seepage field control equation is written as

$$\nabla[-\delta_k K/(\rho_1 g)(\nabla p + \rho_1 g \nabla z)] = \delta_Q Q_s, \tag{3}$$

where ρ_1 denotes the density of fluids; K is the permeability of rock; Q_s represents the source and sink of fluids; p is the pore water pressure; and δ_k and δ_Q denote the flux and source proportion coefficient, valued as 1.0.

The change in the porosity of rock under the effects of different loads and the change in the seepage channel induced by rock damage were jointly used to characterize the change in the fluidity of fluids in rocks. On this basis, a rock stress-seepage-damage multifield coupled constitutive relationship was established [20]

$$K = K_0(\phi/\phi_0)^3 \exp(\alpha_k D), \tag{4}$$

where K_0 denotes initial permeability of rock, ϕ represents the porosity of the rock, ϕ_0 is the initial porosity of the rock, and α_k represents the coefficient of influence of damage on the permeability of solid media, which is set to 5.

The total stress of rock is jointly contributed by the effective stress borne by skeleton grains and pore water pressure. The principle for the effective stress of porous media is expressed as

$$\sigma_{ij}{}^* = \sigma_{ij} - \alpha\delta_{ij}p, \tag{5}$$

where $\sigma_{ij}{}^*$ is the effective stress tensor; σ_{ij} denotes the total stress; α is the equivalent pore water pressure coefficient; and δ_{ij} denotes the Kronecker symbol.

Hence, the constitutive relationship for the stress-strain elastoplastic damage of surrounding rocks under a high seepage pressure field is presented as follows:

$$\sigma_{ij}^* = C_d^e : \left(\varepsilon_{ij} - \varepsilon_{ij}^p\right), \tag{6}$$

where ε_{ij} is the total strain tensor, ε_{ij}^p denotes the plastic strain tensor, and C_d^e represents the damage elasticity matrix. In $C_d^e = 2G_d I + K_d I \otimes I$, I is a symmetric fourth-order tensor. In $I_{ijkl} = 1/2(\delta_{ik}\delta_{jl} + \delta_{il}\delta_{jk})$, G_d and K_d represent shear modulus and volume modulus of damage, respectively, which can be expressed by G_0 and K_0.

$$G_d = (1-D)G_0 = \frac{E(D)}{2(1+\mu)}; K_d = (1-D)K_0 = \frac{E(D)}{3(1-2\mu)}. \tag{7}$$

2.2. Numerical Model of the North Tianshan Karst Tunnel. The burial depth of a karst tunnel section for the North Tianshan Tunnel is about 1000 m. The rocks surrounding the tunnel are mainly composed of limestone mixed with clastic rock, and the groundwater is karst fracture water. The tunnel section studied is situated at the wing of the anticline. There is a karst cave with a diameter of about 10 m and a water pressure of 10 MPa located 10 m from the tunnel boundary. The tunnel face is horseshoe-shaped with dimensions of 9 m × 12 m. In the numerical calculation process, the tunnel shape was simplified into a circle. Given that the diameter of the tunnel face in practical engineering was set to 10 m, as shown on the left, and the karst cave in its natural state exhibits complex shapes, the shape of the karst cave was also simplified into a circle with a diameter of 10 m, as illustrated in the right; the distance between the karst cave and tunnel boundary was 10 m.

To analyze the coupled characteristics of damage to and seepage of surrounding rocks in the tunnel blasting excavation process, the modeling process did not consider the effect of stress concentration in the karst cave on the damage evolution of surrounding rocks and regarded the karst cave that possesses mechanical properties of surrounding rocks as the source of high-pressure water sources. The COMSOL Multiphysics was used to establish a two-dimensional model measuring 100 m × 100 m (width × height), as shown in Figure 1.

The calculations are finished in two steps: in the first step, static force calculations are conducted to derive the geostress field and water pressure field prior to tunnel excavation; in the second step, the geostress and water pressure calculated in the first step are taken as initial values to perform the dynamic calculation of blasting excavation.

(1) Seepage boundary conditions

When calculating static stress, according to practical engineering conditions and considering the karst cave bore a large water pressure, its gravity gradient was neglected; the water pressure of the karst cave was set to 10 MPa, the water pressure on the external boundaries of the model was set to 0.5 MPa so as to simulate the surrounding flow field, while dynamic stress arising from blasting excavation was calculated by setting 0 MPa water pressure on the tunnel boundary and other conditions keeping unchanged.

(2) Displacement and stress boundary conditions

Existing research on stress distribution in deep rocks of China reveals that when the burial depth was 1000 m, vertical geostress was about 20 MPa and horizontal geostress was 20 MPa [21]. During the calculation of static stress, the stresses on the right boundary and upper boundary of the model were set to 20 MPa, while the normal displacements on the left and bottom boundaries of the model were restricted. When calculating the dynamic stress induced by blasting excavation, the external boundary conditions were unchanged, but the effect of blasting on surrounding rocks was simulated using an equivalent loading mode on the

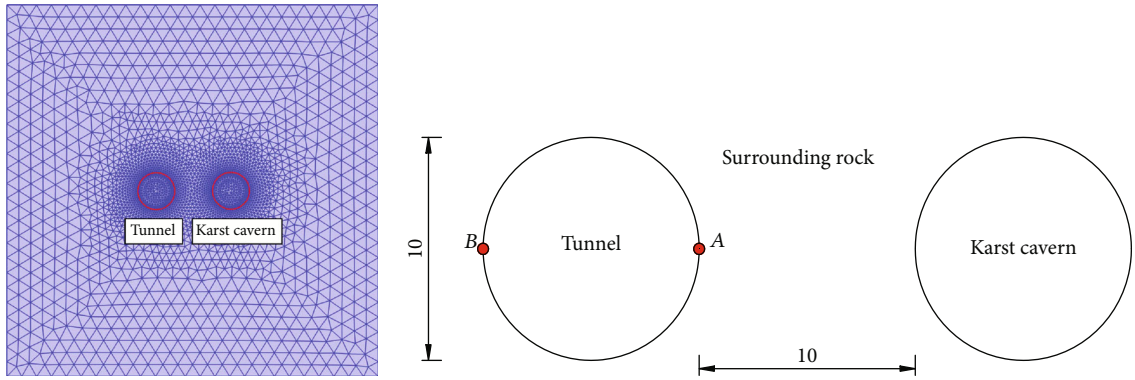

(a) Model grid division

(b) Tunnel and karst cave layout (unit: m)

Figure 1: Two-dimensional geometric model.

Table 1: Blasting parameters.

P_{ej}(kg/m^3)	D/m/s	D_{cj}mm	L_{cj}m	D_{bj}mm	L_{bj}m	L/m
1200	3600	32	2	45	2.5	0.9

tunnel boundary in the tunnel excavation section. The load was simplified into a triangular load, and the equivalent load can be calculated using the following equations [22, 23]:

$$P_0 = \frac{\rho_e D^2}{2(\gamma+1)}\left(\frac{d_c}{d_b}\right)^{2\gamma}\left(\frac{l_c}{l_b}\right)^{\gamma}\cdot n,$$
$$P_e = \frac{d_b}{L}P_0, \tag{8}$$

where P_0 is the peak load of the hole wall of the tunnel; ρ_e refers to the explosive density; D denotes the detonation velocity of explosive; d_c and l_c represent the diameter and length of the explosive package; d_b and l_b refer to the diameter and length of a blasting hole; γ is the entropy of explosive, which is set to 3; n denotes the pressure increment coefficient, valued as 8; P_e represents the equivalent peak load; and L is the distance between blasting holes. The blasting parameters are shown in Table 1.

The equivalent peak load was calculated to be 50 MPa, which was applied on the tunnel boundary. The blasting load curve is shown in Figure 2.

The material parameters of saturated limestone surrounding the karst section of the North Tianshan tunnel were chosen, as listed in Table 2.

2.3. Tunnel Blasting Excavation-Induced Damage and Seep Characteristics of Surrounding Rocks. Figure 3(a) displays the nephogram of water pressure distribution on surrounding rocks before tunnel blasting excavation (the water pressure on the boundary of the karst cave is 10 MPa). It can be found that with the increasing distance between the karst cave and the tunnel boundary, water pressure on the surrounding rock uniformly decreases. This causes uneven distribution of water pressure on the rocks surrounding the tunnel: the water pressure on the surrounding rocks on the right side of the tunnel near the karst cave is large, while the water pressure on the surrounding rocks on the left side which is far away from the karst cave is small.

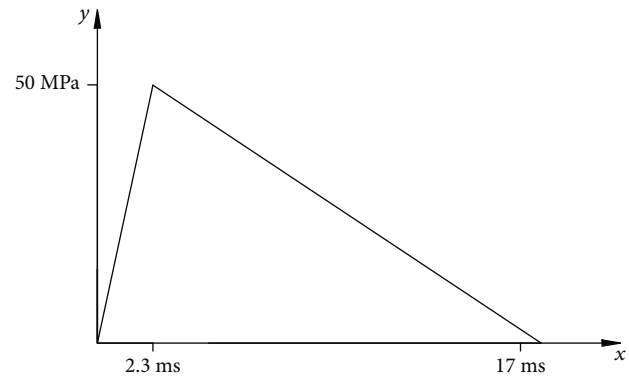

Figure 2: Time history curve of explosion load.

The distribution of the surrounding rock damage in the tunnel after stable excavation in the case of inconsistent water pressures is presented in Figure 3(b). The range of damage to surrounding rocks on the left side of the tunnel is 1.83 m, while that of the right side of the tunnel is slightly large, which is 2.23 m.

To compare the differences in the changes in the damage of surrounding rocks on the left and right sides of the tunnels as well as the influence of water pressure on the damage evolution, measurement point A in the right-side wall and measurement point B in the left side wall of the tunnel were monitored, as shown in Figure 1(b). On this basis, the time-history curve of the damage variable of surrounding rocks, and water pressure in the tunnel blasting excavation process is plotted, as illustrated in Figure 4. The damage changes in measurement points A and B implied that damage to surrounding rocks mainly occurs at the moment that tunnel

Table 2: Rock material parameters.

Density (kg/m^3)	Elastic modulus (GPa)	Compressive strength (MPa)	Poisson ratio	Force of cohesion (MPa)	Angle of internal friction (°)	Initial permeability (m^2)	Original porosity
2600	40	102	0.22	5	50	10^{-12}	0.05

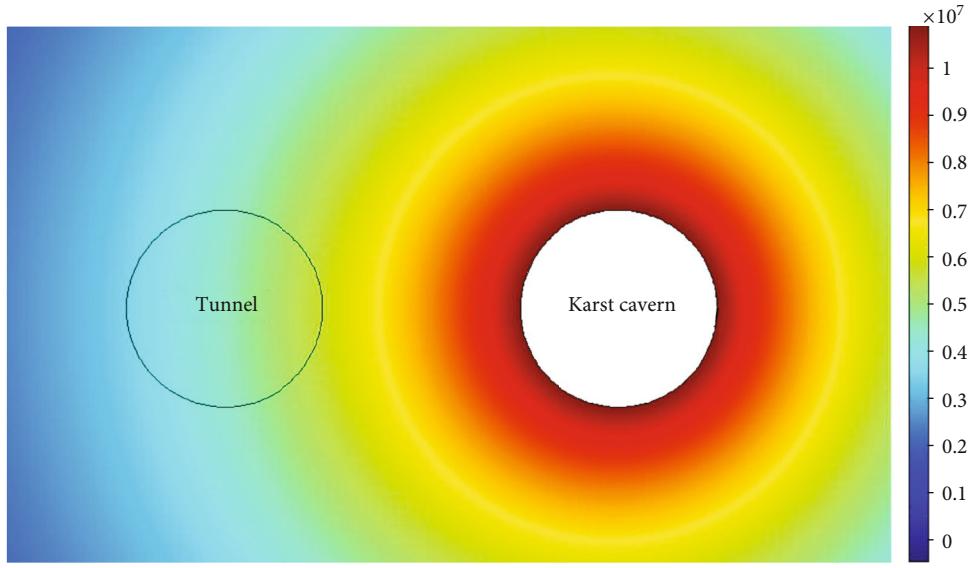

(a) Water pressure distribution (unit: MPa)

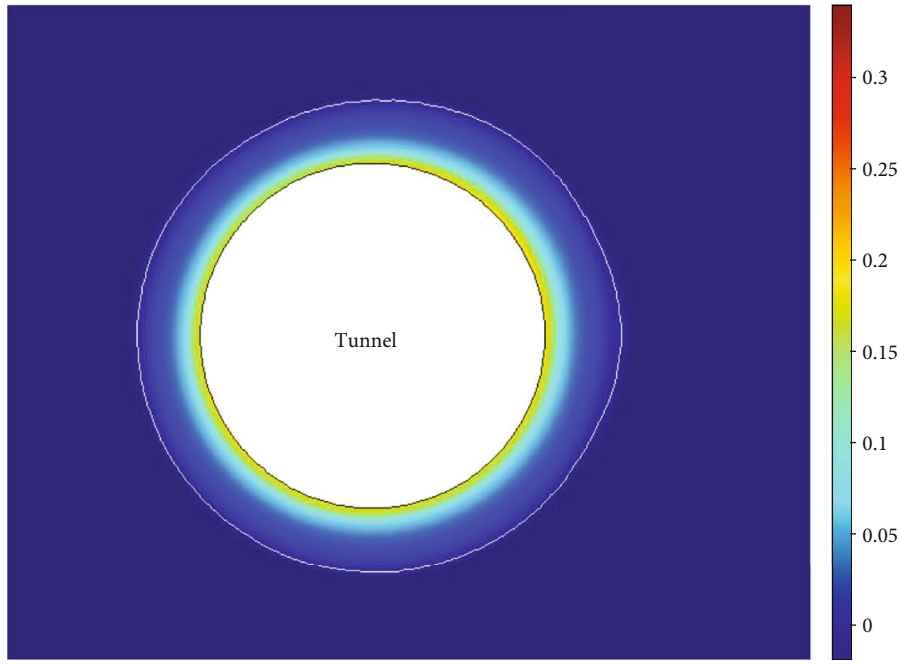

(b) Damage distributions

Figure 3: Water pressure distribution of tunnel before excavation and damage of surrounding rock in the stable stage.

excavation beings. The damage variable time-history curve shows a step-like increase: the increasing stage in the first step is found to be the blasting load impacting stage, corresponding to the peak stage of the load curve in Figure 2. The blasting load exerts a huge impact on surrounding rocks, which induces damage, namely, called blasting-induced damage; the damage at the second step occurs after the impact of the blasting load is fulfilled. At this moment, the tunnel excavation has been completed and forms a free face. The initial geostress on the tunnel profile section in

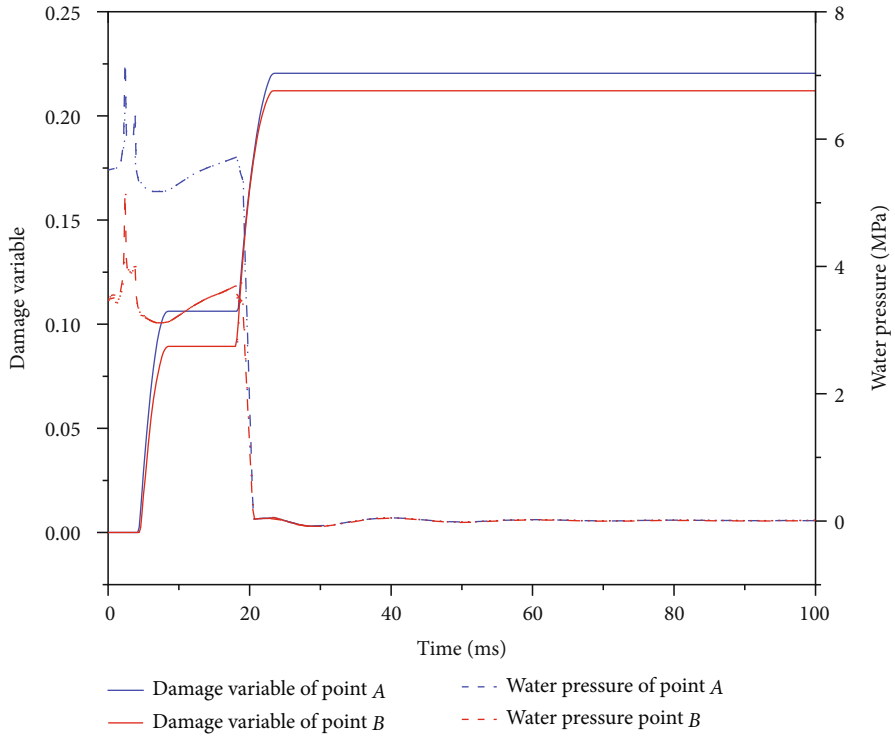

Figure 4: Time history curves of damage variable and water pressure at points A and B.

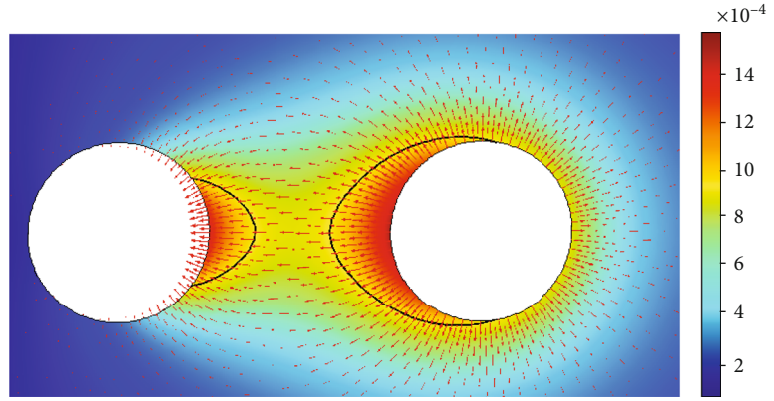

Figure 5: Velocity field distribution of surrounding rock after excavation (unit: m/s).

the normal direction and the effect of impact extrusion induced by blasting loads disappear instantly, namely, the effect of transient unloading acts, which leads to secondary damage to surrounding rocks. This consequently causes the generation of the second step, which occurs after 17 ms in the loading curve shown in Figure 2. Finally, the damage variable (called unloading-induced damage) measured at measurement point A is 0.22, while the damage variable at measurement point B is 0.21. In other words, the damage of surrounding rock is composed of two parts: explosion load and transient unloading of ground stress and the dynamic response caused by transient unloading always lags behind the explosion load, which is consistent with the research results of Lu et al. [24]. Measurement point A has larger damage than measurement point B, which is because A is subjected to a larger influence from the seepage field compared with B in the blasting excavation process. As can be seen from Figure 4, before blasting excavation, measurement point A suffers a larger water pressure, which leads the pore water pressure in rock mass to increase sharply in the blasting excavation stage. This is conducive to the propagation of cracks in rock masses, further causing damage to surrounding rocks, while the peak water pressure of measurement point A is higher than that of B at the blasting excavation stage, thus resulting in larger damage.

Figure 5 displays the nephogram of the flow velocity field distribution of surrounding rocks after excavation. Karst water seeped into the surrounding zones of the karst cave;

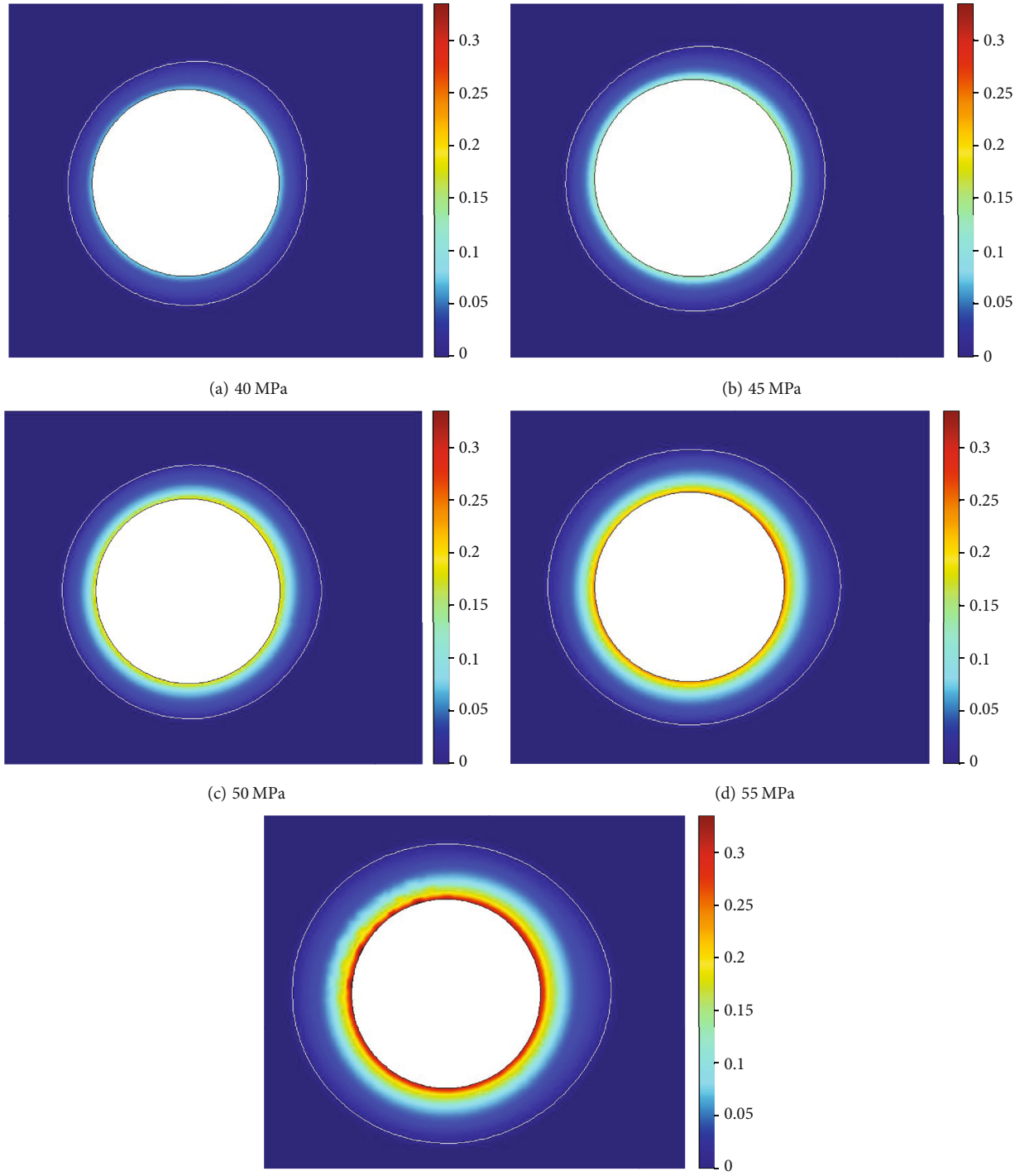

(a) 40 MPa

(b) 45 MPa

(c) 50 MPa

(d) 55 MPa

(e) 60 MPa

Figure 6: Damage of surrounding rock after excavation under different explosion loads.

however, due to the small distance between the right boundary of the tunnel and the karst cave and the larger damage caused by the coupled effects of blasting excavation and seepage field, the cracks in rock masses develop, which provides more seepage channels. The curve in the figure is the isoline at a flow velocity of 1×10^{-3} m/s. Karst water seepage is mainly concentrated on the right boundary of the tunnel. The process of crack initiation, propagation, and coalescence in the surrounding rock caused by karst tunnel excavation and finally forming a water inrush channel connecting the water source and the roadway fracture surface is basically consistent with the research results of Li et al. [25].

Based on the analysis aforementioned, the surrounding rock damage in the karst tunnel excavation process consists

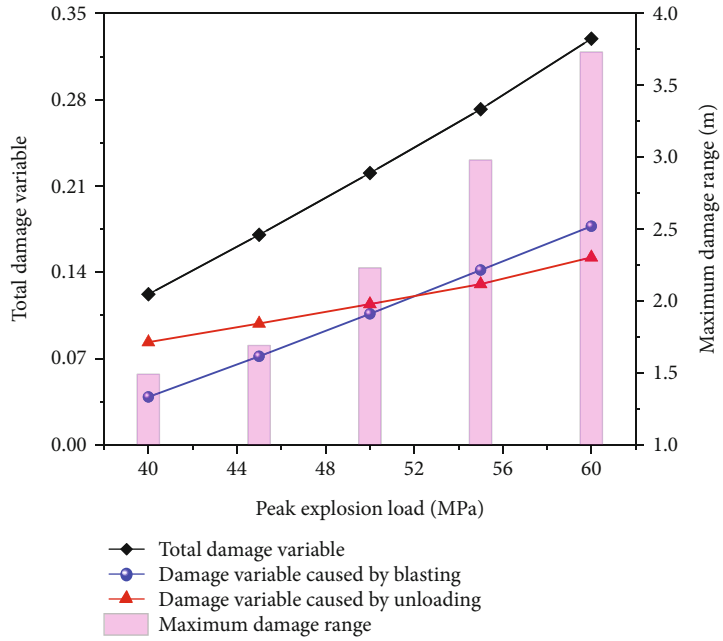

Figure 7: Damage of surrounding rock under different explosion loads.

of blasting-induced damage and unloading-induced damage. After the blasting excavation, the water pressure on the karst cave and damage state of the surrounding rocks of the tunnel also influence the distribution of the seepage field in the surrounding rocks after excavation. Furthermore, blasting load, geostress, and water pressure can directly affect the distribution of the surrounding rock damage. To expound the blasting excavation-induced damage and seepage characteristics of surrounding rocks in the tunnel under multifield coupled effects, the interactive relationship of damage field and seepage field was studied by adjusting the values of the influencing factors including blasting load, geostress, and water pressure on the karst cave.

3. Influencing Factors of the Damage and Seepage Characteristics of Surrounding Rocks

3.1. Influence of Blasting Load. As the blasting load directly acts on the excavation boundary during the tunnel blasting excavation process, the explosive loading degree can exert a direct influence on the degree of damage to surrounding rocks. The damage characteristics of surrounding rocks under different explosive loads (40, 45, 50, 55, and 60 MPa) and the relationship between the damage of surrounding rocks and the seepage field were investigated. Figure 6 displays the nephogram of damage of surrounding rocks after excavation under different explosive loads. With the increase of explosive peak load, the damage to surrounding rocks intensifies, and cracks are therefore more developed, which promotes the flow of high-pressure water in surrounding rocks. Under the effect of water pressure, the damage to surrounding rocks further increases, which makes the range of the damage zone of surrounding rocks at the right-side wall gradually exceed that at the left-side wall. The damage zone protrudes to the right.

In addition, changes in the damage variable at measurement point A and the maximum damage range of surrounding rocks on the right side of the tunnel can be used to characterize the influence of varying explosive loads, as shown in Figure 7. As illustrated in the figure, the total damage variable at measurement point A shows an approximately linear increase with increasing explosive load; the larger the explosive load, the larger the blasting-induced damage and unloading-induced damage. The damage range presents an accelerating increase.

The change in the seepage zone with a flow velocity above 1×10^{-3} m/s can be intuitively describe by the flow velocity field distribution, denoted as "seepage zone A", which is shown as the zone surrounded by isoline in Figure 8.

As the explosive load ingresses, the ranges of the tunnel and the seepage zone A located near the karst cave both show increasing enlargement and tend to coalesce; when the explosive load reaches 60 MPa, the right and left sides of seepage zone A coalesce. Figure 9 depicts the changes in flow velocity at measurement point A after excavation under different explosive loads. The explosive load increases from 40 MPa to 60 MPa. The flow velocity at measurement point A increases from 1.26×10^{-3} m/s to 1.39×10^{-3} m/s, presenting an increasing amplitude.

3.2. Influence of Geostress. The presence of the gravity effect of upper strata endows deeply buried rock mass with a larger initial geostress, which coupled with the effect of transient unloading induced by tunnel excavation to further triggers changes in the damage field and seepage field of surrounding rocks. Through establishing tunnel excavation models under different geostress conditions (10 MPa, 15 MPa, 20 MPa,

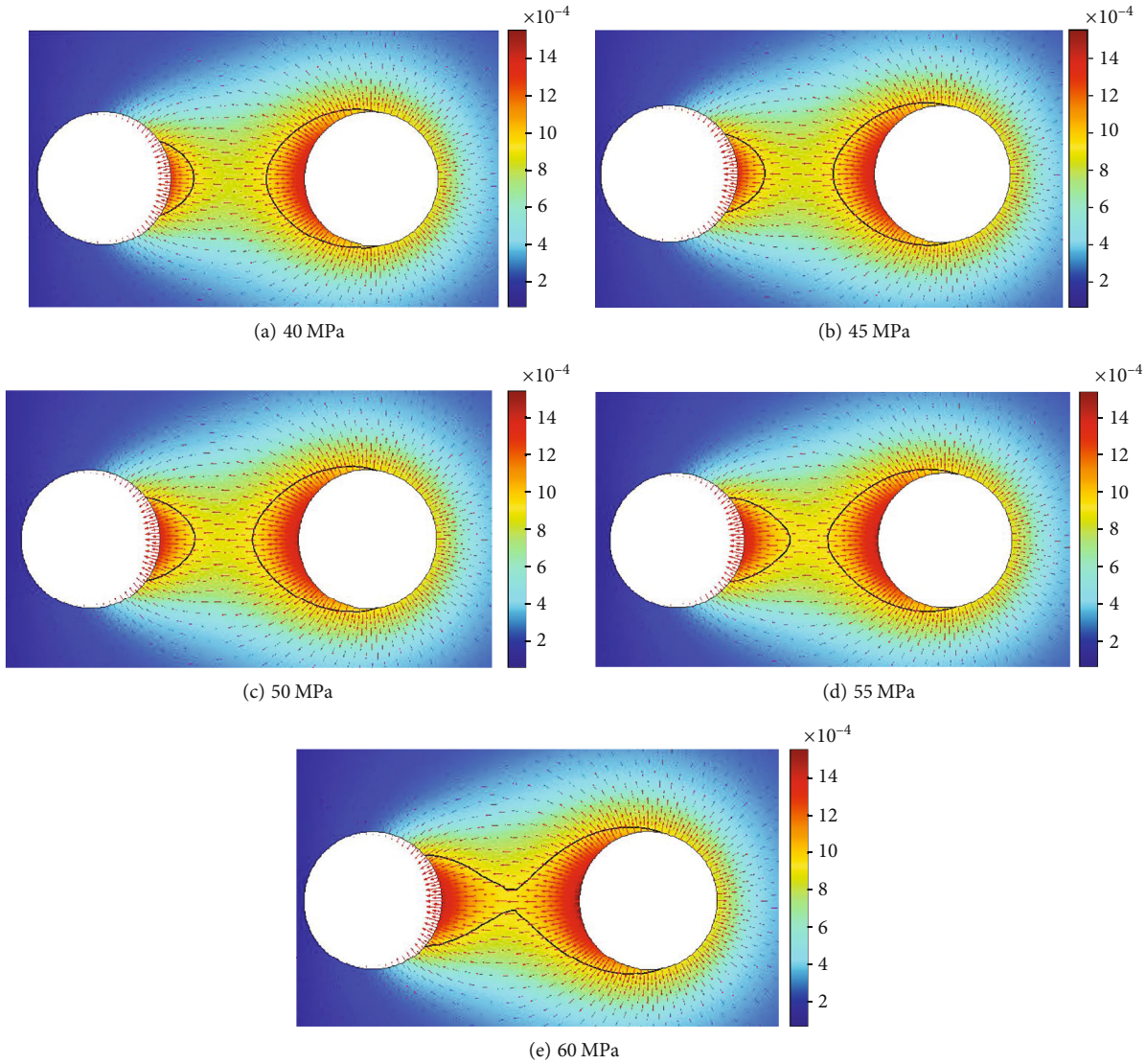

Figure 8: Velocity distribution after excavation of different explosion loads (unit: m/s).

25 MPa, and 30 MPa), the influences of geostress on the damage field and seepage field of surrounding rocks after tunnel excavation were estimated.

Figure 10 presents the nephogram of damage for surrounding rocks after blasting excavation under different geostress conditions. When geostress is too small, the damage zone protrudes towards the karst cave, while with the enhancement of geostress, surrounding rocks are located in a more compact state, and crack closure of surrounding rocks appears. Seepage pressure exerts a smaller effect compared with geostress, so the joint effect of damage and seepage reduces. The damage zone tends to be annularly distributed.

As shown in Figure 11, the change in geostress leads to obvious changes in the range of the damage zone and damage degree. The relationship between geostress, the range of the damage zone, and the damage degree can be characterized by the changes in the damage variable at measurement point A and the maximum damage range at the right side of the tunnel, as displayed in Figure 11. With the increase in

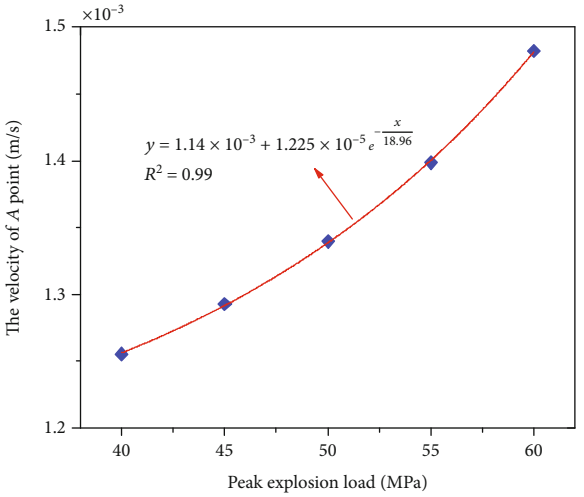

Figure 9: The relationship between the velocity change of point A and the explosion load.

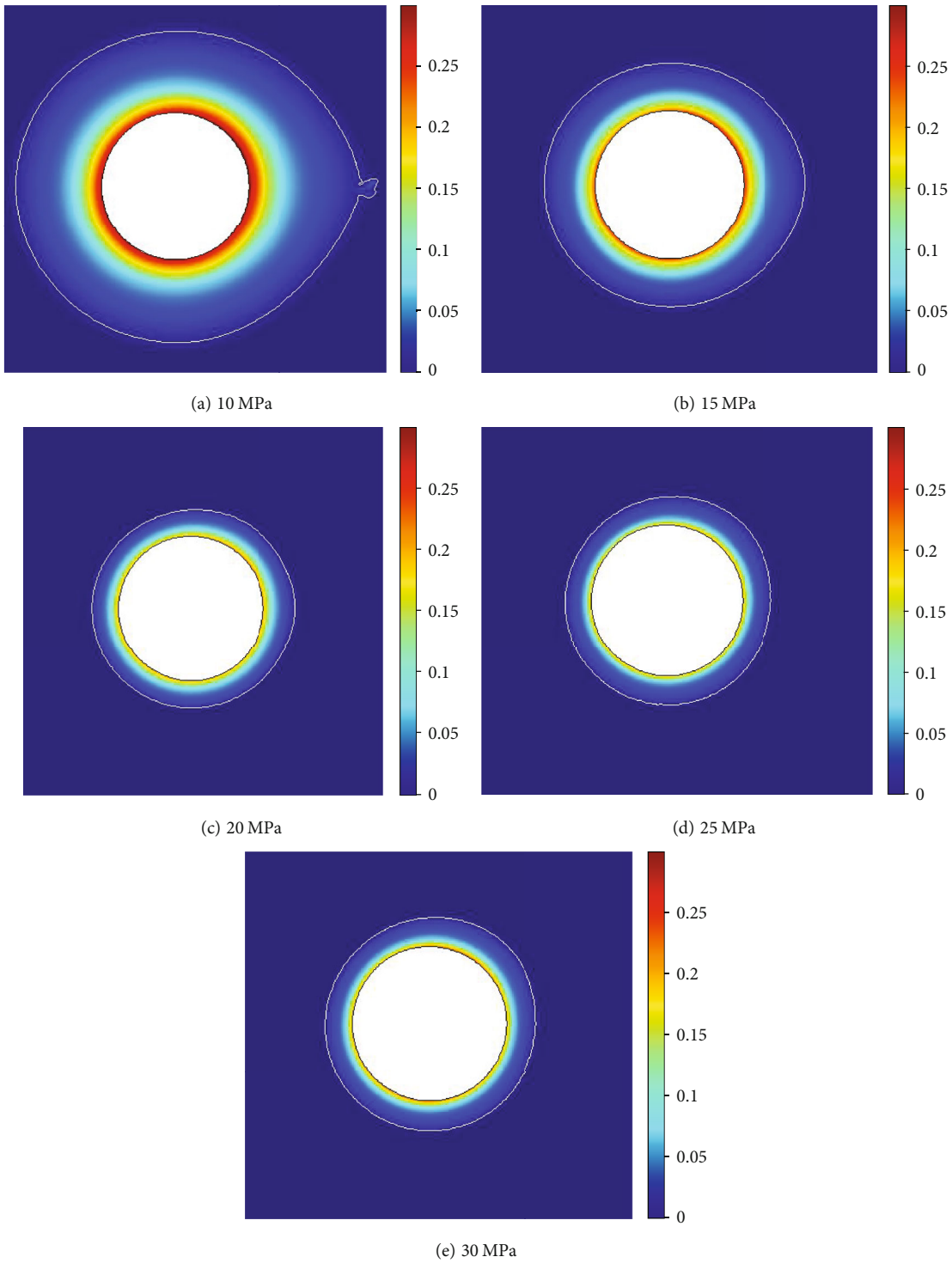

Figure 10: Distribution of surrounding rock damage after excavation under different geostress.

geostress, blasting-induced damage diminishes gradually, while unloading-induced damage increases little by little. When geostress is above 20 MPa, unloading-induced damage is higher than blasting-induced damage. In the process that geostress is increasing to 25 MPa, total damage, and damage range keep continues to increase. As geostress increases from 25 MPa to 30 MPa, total damage, and damage range show a small amplitude of increase.

Figure 12 demonstrates the nephogram of the flow velocity distribution after excavation under different geostresses. When geostress is too small, seepage zone A realizes the coalescences between the karst cave and the tunnel from left to right. With the increase of geostress, the range of seepage zone A continues to shrink. When geostress reaches 20 MPa, the left-to-right coalescence of seepage zone A is broken off. In the case that geostress increases from 25 MPa

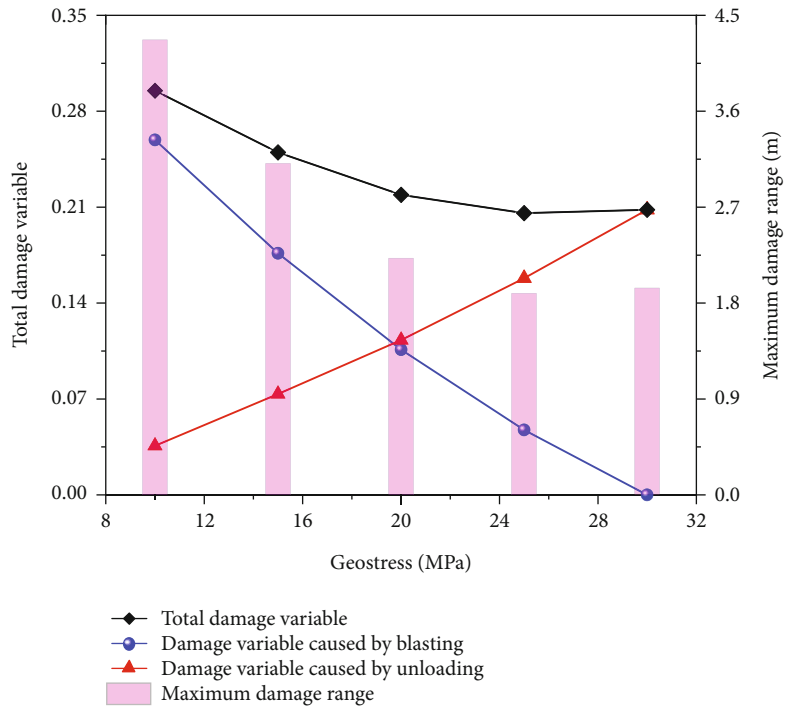

Figure 11: Damage of surrounding rock after excavation in different geostress.

to 30 MPa, the range of seepage zone A begins to enlarge in a small amplitude.

Figure 13 exhibits the change in flow velocity at measurement point A of the tunnel after excavation under various geostresses. As geostress increases from 10 MPa to 25 MPa, the flow velocity at the right-side wall of the tunnel decreases from 1.70×10^{-3} m/s to 1.30×10^{-3} m/s; when geostress increases to 30 MPa, the flow velocity again increases to 1.31×10^{-3} m/s.

3.3. Influence of Water Pressure on the Karst Cave. Different water pressures of the karst cave are prone to cause differences in seepage pressures of surrounding rocks. This affects both the damage and crack opening processes of surrounding rocks during the tunnel excavation process, finally influencing the seepage field distribution of surrounding rocks. By establishing the tunnel excavation models under different water pressures (0 MPa, 5 MPa, 10 MPa, 15 MPa, and 20 MPa) of the karst cave, the influences of the water pressure in the karst cave on damage field and seepage field distribution of surrounding rocks after excavation were investigated.

Figure 14 demonstrates the nephogram of the surrounding rock damage after excavation under different water pressures in the karst cave. When the water pressure in the karst cave is 0 MPa, the seepage conditions surrounding the left and right sides of the tunnel are the same, and the damage zone of surrounding rocks is shown to be annularly distributed; however, with the increase in the water pressure of the karst cave, the damage zone protrudes to the right side. This is because, with the increasing water pressure of the karst cave, the surrounding rocks at the right-side wall of the tunnel suffer the increasing effect of high seepage pressure, which promotes the openness and development of cracks on surrounding rocks. As a result, large damage occurs to surrounding rocks. The range and degree of the damage of surrounding rocks at the boundary of the tunnel increase with rising water pressure of the karst cave.

The relationship between the water pressure in the karst cave, the range, and the degree of damage can be characterized by the changes in the damage variable at measurement point A and the maximum damage range at the right side of the tunnel, as shown in Figure 15. Increasing water pressure in the karst cave can intensify blasting-induced damage and reduce unloading-induced damage. Its effect on the blasting-induced damage is shown to be larger, making the total damage at measurement point A, and the damage range of surrounding rocks larger.

Figure 16 is the nephogram of the flow velocity distribution after excavation under different water pressures in the karst cave. When the water pressure in the karst cave is small, there is no obvious seepage phenomenon in the surrounding rocks. As the water pressure reaches 10 MPa, seepage zone A appears, and its range rapidly enlarges with a small increase of the water pressure. When the water pressure lives up to 15 MPa, seepage zone A between the karst cave and the tunnel coalesces.

Figure 17 shows the change in flow velocity at measurement point A after excavation under different water pressures in the karst cave. When the water pressure in the karst cave increases from 0 MPa to 20 MPa, the flow velocity at measurement point A nearly increases from 0 to 3.1×10^{-3} m/s; the flow velocity exhibits an approximately linear increase with water pressure.

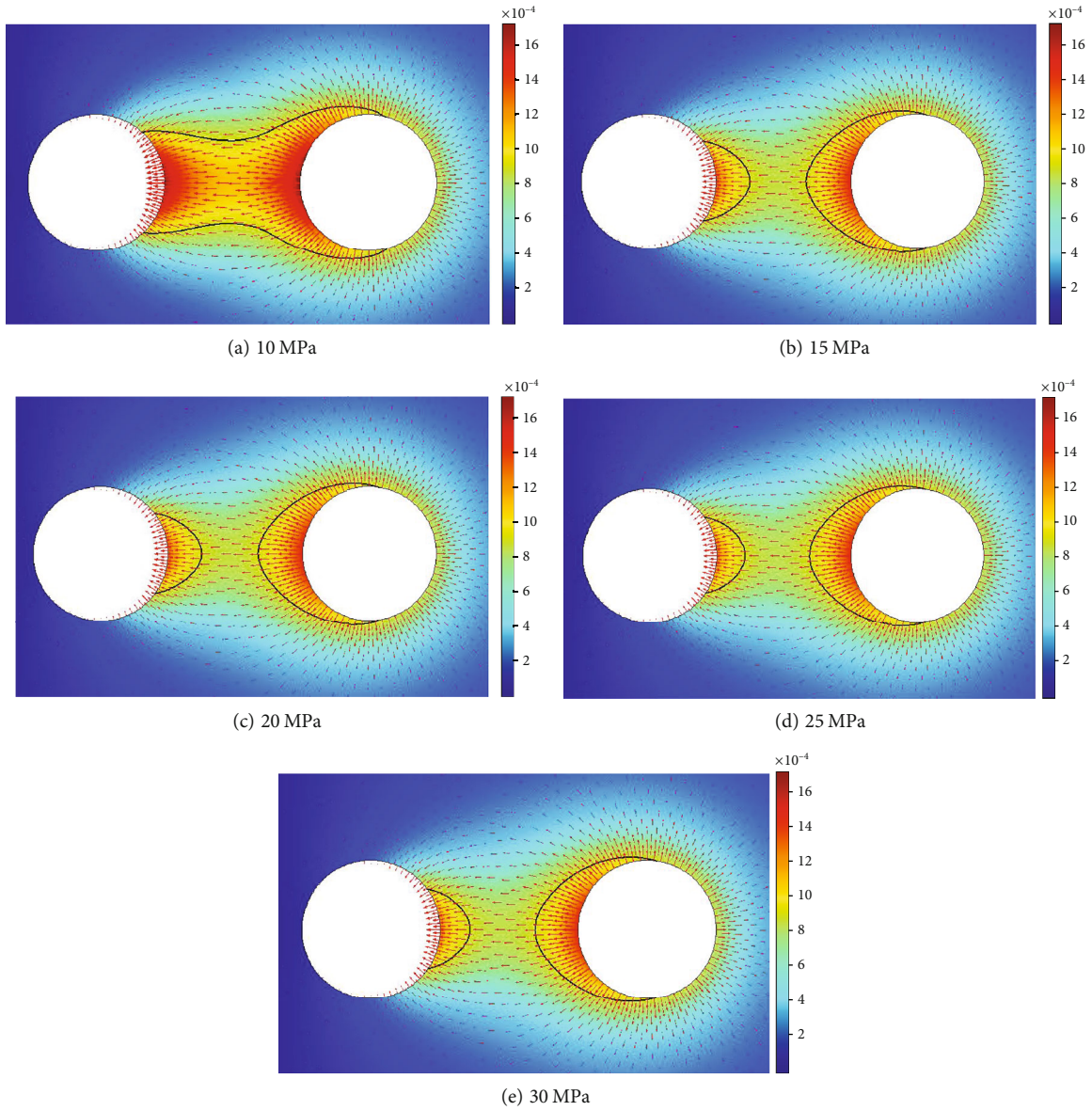

Figure 12: Velocity distribution of surrounding rock after excavation under different geostress (unit: m/s).

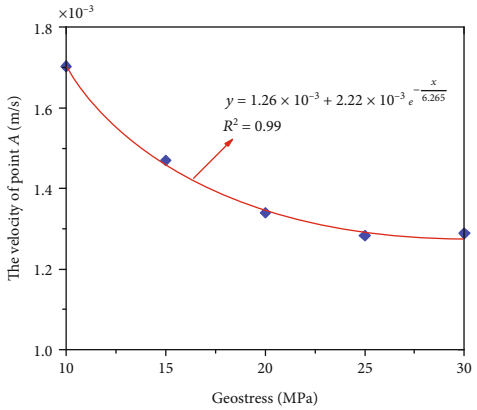

Figure 13: The relationship between the velocity change of point A and the geostress.

3.4. Interactive Relationship between the Damage Field and Seepage Field. The analysis aforementioned has demonstrated the damage field and seepage field distribution characteristics of surrounding rocks after blasting excavation under different explosive loads, geostresses, and water pressures in the karst cave. The analysis results indicate that water pressure has an important effect on the damage distribution of surrounding rocks during the excavation process. Meanwhile, the blasting excavation process can cause a change in pore water pressure and thus affect the distribution of the damage field. The damage effect will further lead the surrounding rock cracks to develop, inducing expansion of the seepage channels, and consequently changing the flow velocity in surrounding rocks. The relationship between the damage at measurement point A (and the damage range on the right sides of the tunnel) and flow velocity is shown in Figure 18.

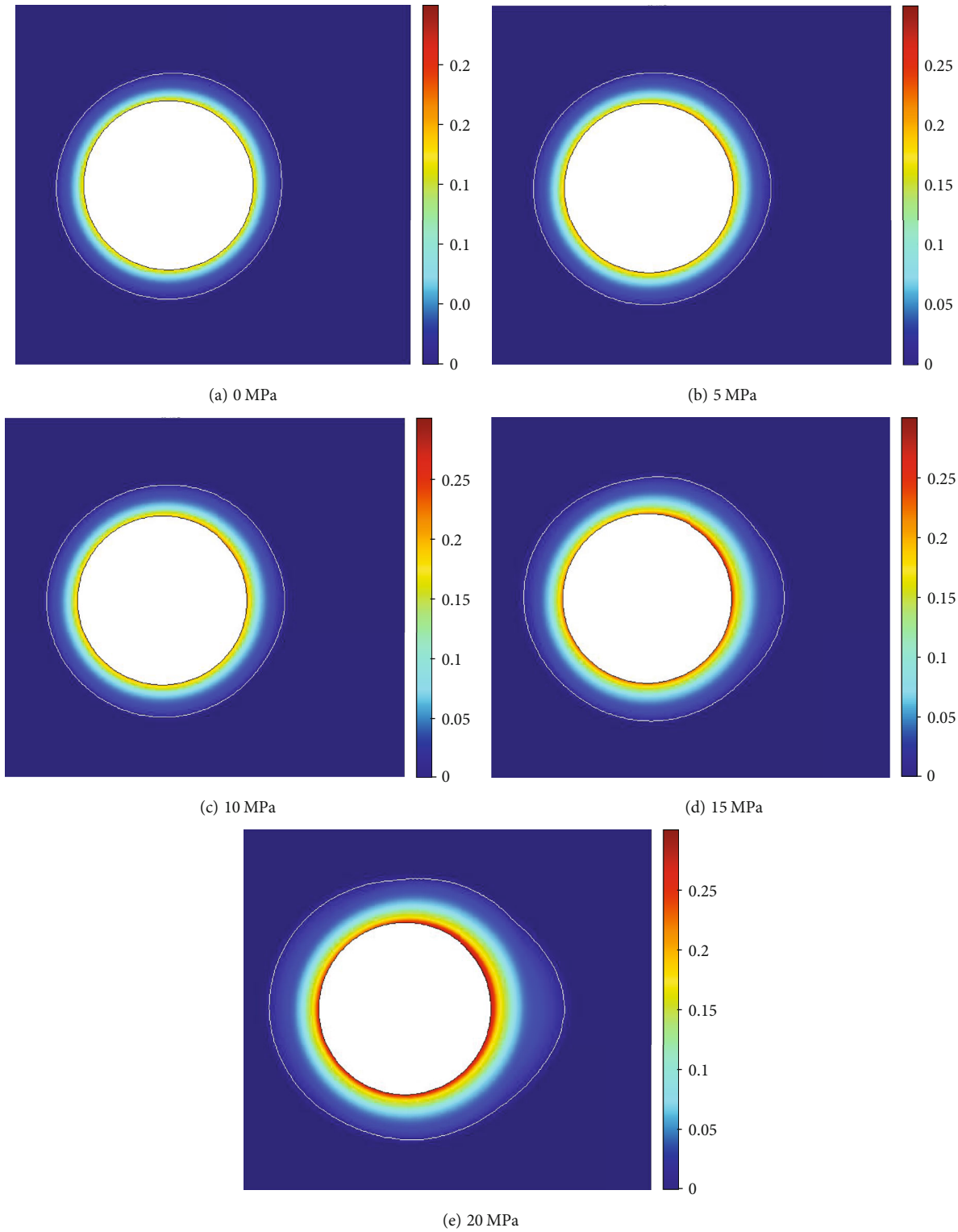

Figure 14: Damage distribution of surrounding rock after excavation under different water pressures.

The calculation results under different explosive loads and geostresses indicate that the increases in the range and degree of damage can increase the flow velocity in surrounding rocks. Under varying water pressures, according to Darcy's law, increasing water pressure in the karst cave can directly increase the flow velocity of surrounding rocks around the tunnel and cause increasing damage while indirectly inducing rising flow velocity. Meanwhile, according to Bernoulli's equation, changes in the flow velocity of surrounding rocks also cause a change in water pressure, which further affects the damage field distribution. Such a complex coupled effect leads to the formation of a seepage field and

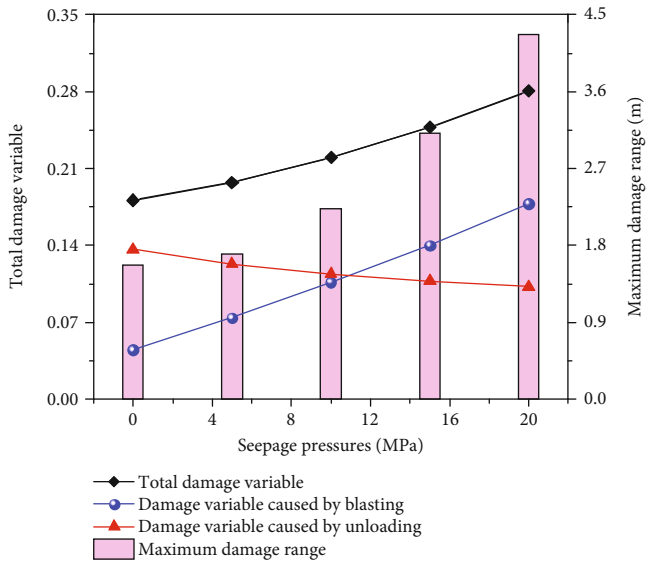

Figure 15: Damage of excavation surrounding rock under different water pressure of karst cave.

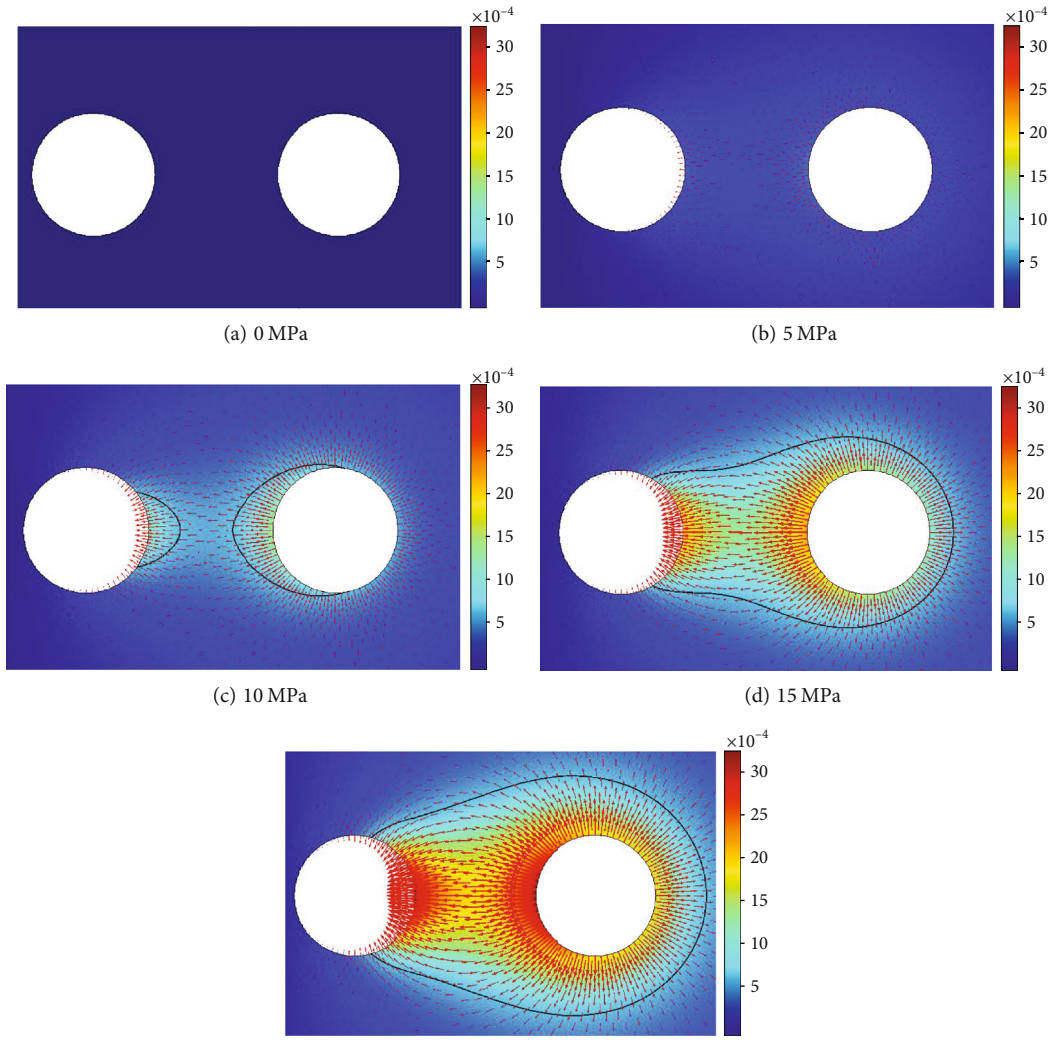

(a) 0 MPa

(b) 5 MPa

(c) 10 MPa

(d) 15 MPa

(e) 20 MPa

Figure 16: Velocity distribution of different karst caves after water pressure excavation (unit: m/s).

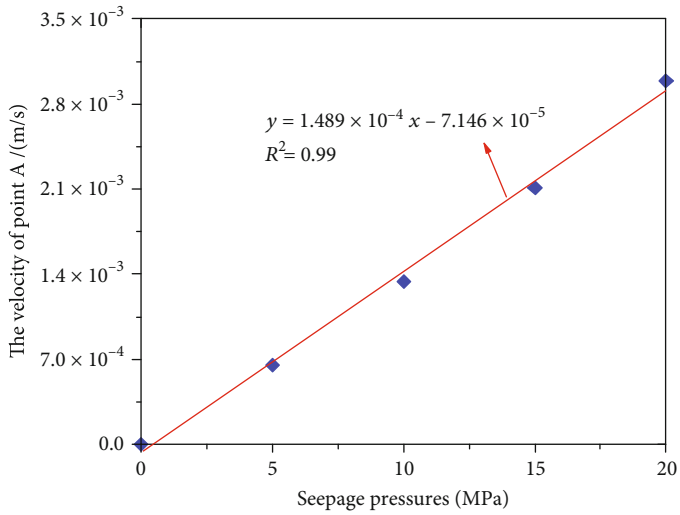

Figure 17: The relationship between the velocity change of point A and water pressure of karst cave.

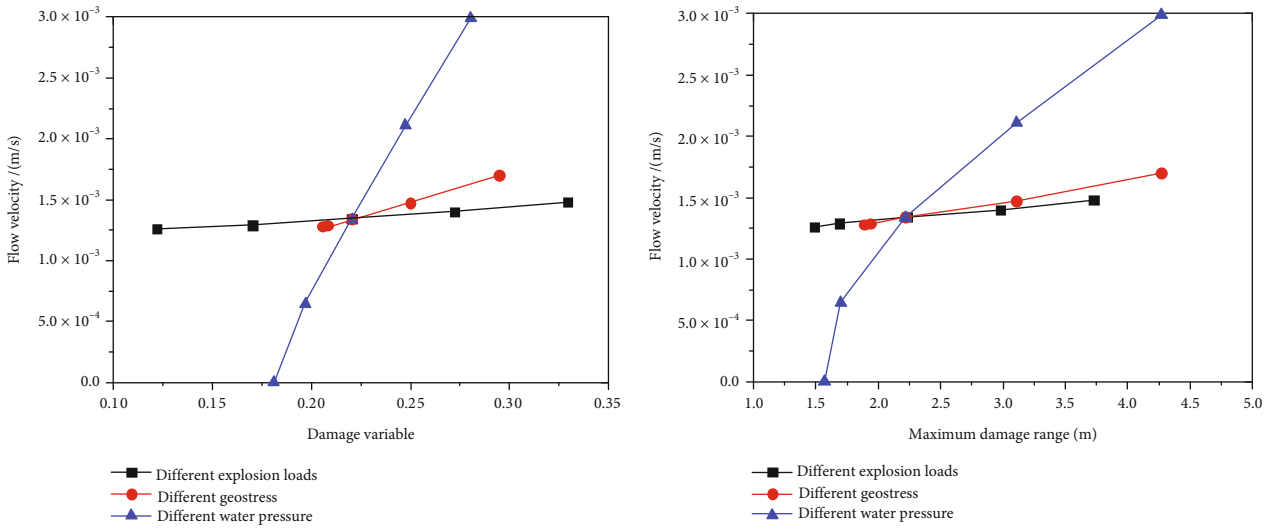

(a) Damage variable

(b) Maximum damage range

Figure 18: Relation curve between velocity and damage of measuring point A.

damages the field distribution of surrounding rocks after excavation.

4. Conclusion

This research took the blasting excavation of a deeply buried karst tunnel in the North Tianshan Mountains in China as research object. On this basis, a multifield coupled model for blasting excavation in the deeply buried rock tunnel was established to explore the damage induced by blasting excavation in the karst tunnel and the seepage characteristics of surrounding rocks under high geostress. The conclusion can be drawn as follows:

(1) Damage of surrounding rocks is attributed to the joint effects of blasting impact and transient unloading of geostress. The damage variable time-history curve shows a step-like increase: the increasing stage in the first step is found to be the blasting load impacting stage (blasting damage stage); the damage at the second step occurs after the impact of blasting load is fulfilled (unloading damage stage). The increase of geostress can weaken the blasting-induced effect on rock mass while enhancing the unloading-induced damage to rock mass; when geostress is above 20 MPa, unloading-induced damage is higher than blasting-induced damage; the increases in water pressure of karst caves can reduce unloading-induced

damage to rock while strengthening blasting-induced damage to rock

(2) The increases in blasting load and water pressure of karst caves are prone to cause increases in the degree and range of damage to surrounding rocks, while also leading to the increasing flow velocity of karst water between the tunnel and the karst cave; when geostress is below 25 MPa, the increasing geostress will decrease the damage to surrounding rocks after blasting excavation and the overall water flow velocity of karst water; however, when geostress exceeds 25 MPa, the enhancement of geostress can increase the surrounding rock damage and the overall water velocity of karst water

(3) In the blasting excavation process of the deeply-buried karst tunnel, there is a strong damage and seepage coupled effect. With further increases in the degree of damage to surrounding rocks and water pressure of karst caves, the coupled effect is enhanced gradually. Meanwhile, the right side (adjacent to the karst cave) of the tunnel exhibits a larger degree and range of damage to surrounding rocks compared with that of the left side. The damage zone protrudes to the right, leading to a greater water flow velocity of surrounding rocks after excavation, and the flow velocity increases nearly linearly with the increase of water pressure. In addition, there is a positive correlation between the damage field and seepage field of the surrounding rock under blasting

Data Availability

Data is available on request.

Conflicts of Interest

We declare that there are no known competing financial interests or personal relationships that could have appeared to influence the work reported in this paper.

Acknowledgments

This work was supported by the National Natural Science Foundation of China (No. 51979208), the Hubei Provincial Key Laboratory of Blasting Engineering, Jianghan University (HKLBEF202005), the Science and Technology Research and Development Program of China National Railway Group Corporation Limited (K2021G024), and the National Key Research and Development Project of China (2021YFC3100804).

References

[1] X. F. Huo, X. Z. Shi, X. Y. Qiu et al., "A study on raise blasting and blast-induced vibrations in highly stressed rock masses," *Tunnelling and Underground Space Technology*, vol. 123, article 104407, 2022.

[2] Y. Luo, G. Wang, X. Li et al., "Analysis of energy dissipation and crack evolution law of sandstone under impact load," *International Journal of Rock Mechanics and Mining Sciences*, vol. 132, article 104359, 2020.

[3] C. Zhu, Y. Z. Xu, Y. X. Wu et al., "A hybrid artificial bee colony algorithm and support vector machine for predicting blast-induced ground vibration," *Earthquake Engineering and Engineering Vibration*, vol. 21, no. 4, pp. 861–876, 2022.

[4] F. L. Pellet, M. Keshavarz, and M. Boulon, "Influence of humidity conditions on shear strength of clay rock discontinuities," *Engineering Geology*, vol. 157, pp. 33–38, 2013.

[5] C. Zhu, X. D. Xu, X. T. Wang et al., "Experimental investigation on nonlinear flow anisotropy behavior in fracture media," *Geofluids*, vol. 2019, Article ID 5874849, 9 pages, 2019.

[6] Q. Yin, J. Y. Wu, Z. Jiang et al., "Investigating the effect of water quenching cycles on mechanical behaviors for granites after conventional triaxial compression," *Geomechanics and Geophysics for Geo-Energy and Geo-Resources*, vol. 8, no. 2, p. 77, 2022.

[7] Y. T. Li, B. Zhang, L. Wang, Y. Wu, H. X. Wang, and Z. H. Peng, "Identification of dominant seepage channels in fractured rock masses of underground water–sealed oil storage: a case study," *Bulletin of Engineering Geology and the Environment*, vol. 81, no. 9, p. 357, 2022.

[8] S. B. Tang, J. M. Li, S. Ding, and L. T. Zhang, "The influence of water-stress loading sequences on the creep behavior of granite," *Bulletin of Engineering Geology and the Environment*, vol. 81, no. 11, p. 482, 2022.

[9] D. M. Tan, T. Y. Qi, and Y. C. Mo, "Numerical analysis and research on surrounding rock stability of lateral karst cave tunnel," *Chinese Journal of Rock Mechanics and Engineering*, vol. 28, no. S2, pp. 3497–3503, 2009.

[10] L. P. Li, W. F. Tu, Z. Q. Zhou, S. S. Shi, M. G. Zhang, and Y. X. Chen, "Dynamic unloading instability mechanism of underground cavern based on seepage-damage coupling," *KSCE Journal of Civil Engineering*, vol. 24, no. 5, pp. 1620–1631, 2020.

[11] B. Liu, J. L. Li, Q. S. Liu, and X. W. Liu, "Analysis of damage and permeability evolution for mudstone material under coupled stress-seepage," *Materials*, vol. 13, no. 17, p. 3755, 2020.

[12] C. H. Huang, W. H. Dong, Z. Z. Cao et al., "Water inrush mechanism of fault zone in karst tunnel under fluid-solid coupling field considering effective stress," *Geofluids*, vol. 2022, Article ID 4205174, 11 pages, 2022.

[13] H. L. Zhao, F. Zhang, and X. P. Yao, "Hydromechanical simulation of tunnel excavation in rock considering a nearby karst cave," *Mathematical Problems in Engineering*, vol. 2021, Article ID 7875725, 13 pages, 2021.

[14] W. M. Yang, X. Yang, Z. D. Fang et al., "Model test for water inrush caused by karst caves filled with confined water in tunnels," *Arabian Journal of Geosciences*, vol. 12, no. 24, pp. 1866–7511, 2019.

[15] H. Yuan, C. Chen, Z. He, and Y. Wang, "Numerical simulation of fluid-solid coupling in surrounding rock for river stope mining," *Shock and Vibration*, vol. 2020, Article ID 9786182, 11 pages, 2020.

[16] J. Q. Guo, J. X. Chen, F. Chen, Y. B. Luo, and Q. Liu, "Water inrush criterion and catastrophe process of a karst tunnel face with non-persistent joints," *China Journal of Highway and Transport*, vol. 31, no. 10, pp. 118–129, 2018.

[17] Z. Huang, Z. Jiang, S. Zhu, X. Wu, L. Yang, and Y. Guan, "Influence of structure and water pressure on the hydraulic

conductivity of the rock mass around underground excavations," *Engineering Geology*, vol. 202, pp. 74–84, 2016.

[18] Z. Huang, S. Y. Zhu, K. Zhao et al., "Influences of structural variation of host rock induced by engineering activities on water inrush of tunnels," *Chinese Journal of Geotechnical Engineering*, vol. 40, no. 3, pp. 449–458, 2018.

[19] J. X. Wang and A. N. Jiang, "An elastoplastic damage constitutive model of rock and its application to tunnel engineering," *Rock and Soil Mechanics*, vol. 36, no. 4, pp. 1147–1158, 2015.

[20] W. C. Zhu, C. H. Wei, J. Tian, T. H. Yang, and C. A. Tang, "Coupled thermal hydraulic-mechanical model during rock damage and its preliminary application," *Rock and Soil Mechanics*, vol. 30, no. 12, pp. 3851–3857, 2009.

[21] Y. Luo, X. P. Li, P. C. Xu, Q. Dong, and J. S. Hong, "Characteristic study of surrounding rock mass deformation considering accumulative damage effect," *Rock and Soil Mechanics*, vol. 35, no. 11, pp. 3041–3048, 2014.

[22] X. P. Li, B. Wang, and G. L. Zhou, "Reserch on distribution rule of geostress in deep stratumin in Chinese mainland," *Chinese Journal of Rock Mechanics and Engineering*, vol. 31, no. S1, pp. 2875–2880, 2012.

[23] Y. Luo, H. L. Gong, D. X. Qu et al., "Vibration velocity and frequency characteristics of surrounding rock of adjacent tunnel under blasting excavation," *Scientific Reports*, vol. 12, no. 1, p. 8453, 2022.

[24] M. Chen, W. B. Lu, P. Yan, and Y. G. Hu, "Blasting excavation induced damage of surrounding rock masses in deep-buried tunnels," *KSCE Journal of Civil Engineering*, vol. 20, no. 2, pp. 933–942, 2016.

[25] L. P. Li, S. C. Li, S. S. Shi, Z. L. Zhou, M. Guo, and Q. H. Wang, "Multi-field coupling mechanism of seepage damage for the water inrush channel formation process of coal mine," *Journal of Mining and Safety Engineering*, vol. 29, no. 2, pp. 232–238, 2012.